# Choroidal Thickness and Choroidal Vessel Density in Nonexudative Age-Related Macular Degeneration Using Swept-Source Optical Coherence Tomography Imaging

Fang Zheng,[1,2] Giovanni Gregori,[1] Karen B. Schaal,[1] Andrew D. Legarreta,[1] Andrew R. Miller,[1] Luiz Roisman,[1] William J. Feuer,[1] and Philip J. Rosenfeld[1]

[1]Bascom Palmer Eye Institute, University of Miami Miller School of Medicine, Miami, Florida, United States
[2]Department of Ophthalmology, Tianjin Medical University General Hospital, Tianjin, China

Correspondence: Giovanni Gregori, Research Associate Professor of Ophthalmology, Bascom Palmer Eye Institute, 900 NW 17th Street, Miami FL 33136, USA; ggregori@med.miami.edu.

Submitted: June 20, 2016
Accepted: October 23, 2016

Citation: Zheng F, Gregori G, Schaal KB, et al. Choroidal thickness and choroidal vessel density in nonexudative age-related macular degeneration using swept-source optical coherence tomography imaging. *Invest Ophthalmol Vis Sci*. 2016;57:6256–6264. DOI: 10.1167/iovs.16-20161

**Purpose.** To analyze the relationship between choroidal thickness and the distribution of choroidal blood vessels in eyes with nonexudative AMD.

**Methods.** Eyes with a diagnosis of nonexudative AMD were imaged using a prototype 100-kHz swept-source (SS) optical coherence tomography (OCT) instrument (Carl Zeiss Meditec, Dublin, CA, USA) with a central wavelength of 1050 nm. We used an OCT cube scan pattern consisting of 512 × 512 A-scans over a 12 × 12 mm retinal area. The eyes were partitioned into two groups based on the presence or absence of reticular pseudodrusen (RPD). All scans were segmented using an automated algorithm. In addition, five eyes from each of the two groups were randomly chosen for manual segmentation. Binary choroidal vessels maps were generated from suitable OCT choroidal slabs, and the relationship between the density of large choroidal vessels and choroidal thickness was analyzed using an Early Treatment Diabetic Retinopathy Study–like target centered on the fovea.

**Results.** Twenty-five eyes were enrolled in each group. The automated algorithm produced accurate choroidal thickness maps with an average difference between the manual and automated segmentations of 13.7 μm. There was a significant and stable correlation between choroidal thickness and choroidal vessel density across the two groups. Both average choroidal thickness and vessel density were significantly lower in eyes with RPD.

**Conclusions.** Our fully automated choroidal segmentation algorithm was able to capture the different patterns of choroidal thickness over a wide area. Choroidal thickness has a clear relationship with the density of large choroid vessels in our sample, irrespective of the presence or absence of RPD.

Keywords: choroidal thickness, choroidal vessel density, swept-source OCT, nonexudative AMD

The choroid of the eye is a vascular structure that supports the metabolic needs of the RPE and outer retina.[1] Using optical coherence tomography (OCT), it is often possible to visualize the entire choroid and measure its thickness.[2] Over the past several years, a large number of studies have reported on the thickness of the choroid in normal and diseased eyes. Typically, these studies used spectral-domain (SD)-OCT instruments with a central wavelength around 850 nm, adopted a technique called enhanced depth imaging (EDI)-OCT for improved visualization of the choroid, and measured choroidal thickness at a single point under the fovea, or possibly at a few preordained retinal positions.

Choroidal thickness measurements at specific retinal positions exhibit a relatively large test–retest and inter/intragrader variability because the choroidal/sclera interface is often difficult to visualize precisely.[3–5] Despite these limitations, there is a strong negative correlation between subfoveal choroidal thickness measurements and increasing age and axial length in healthy populations.[3,6–8] In a number of disease states, abnormal subfoveal choroidal thickness measurements have been observed. Thicker choroidal measurements have been found in central serous chorioretinopathy, Vogt-Koyanagi-Harada disease, multiple evanescent white dot syndrome, adult onset foveomacular vitelliform dystrophy, and macular telangiectasis type 2.[9–13] Thinner choroid thickness measurements have been observed inferior to the optic nerve,[14] in highly myopic eyes,[15] in diabetic eyes,[16,17] and in eyes with reticular pseudodrusen (RPD), also known as subretinal drusenoid deposits (SDDs).[18–21] In age-related macular degeneration, it is the presence of RPD that has been associated with subfoveal and peripapillary choroidal thinning rather than the diagnosis of AMD.[20,21] After controlling for age and axial length, Thorell et al.[20] showed there was no significant difference between a normal control group and a group of AMD eyes with geographic atrophy (GA) or drusen in the absence of RPD. Rather, it was the presence of RPD that was associated with choroidal thinning. Furthermore, Yiu et al.[22] demonstrated that after adjusting for age and refractive error, central choroidal thickness was not significantly influenced by the diagnosis of AMD status based on AREDS classification.

High-speed swept-source (SS)-OCT imaging with a central wavelength around 1050 nm can provide excellent visualiza-

tion of choroidal vasculature over a wide-field area without the use of EDI. Using SS-OCT, Esmaeelpour et al.[23–25] analyzed the choroidal thickness in healthy eyes, AMD eyes, and eyes with diabetic retinopathy by producing automated choroidal thickness maps over a 36° × 36° field of view. The topographic variance of choroidal thickness over the posterior pole was observed in these choroidal thickness maps. Haas et al.[19] used similar SS-OCT choroidal thickness maps over a 36° × 36° field of view to demonstrate local choroidal thickening underlying RPD within each eye and an overall thinning with respect to eyes with AMD, but without RPD.

In addition to changes in choroidal thickness measurements, the relationship between choroidal vessels and RPD has also drawn some attention. Querques et al.[26] found that the reticular patterns closely abutted, but did not overlie the large choroidal vessels. Grewal et al.[27] showed that RPD appeared to follow the underlying choroidal vasculature. However, Vongkulsiri et al.[28] demonstrated that there is no concordance between SDD and large choroidal vessels or the stroma between these vessels. Mohler et al.[29] generated manual choroidal segmentation over a 60° field and looked at choroidal vascular patterns in nine eyes with and without chorioretinal diseases. In these examples, a possible connection between the geographic distribution of choroidal thickness and the choroidal vascular patterns was suggested.

In the present study, we used a SS-OCT instrument to acquire images over a 12 × 12 mm retinal region, a 40° field of view, and generated choroidal thickness maps using a custom fully automated choroidal segmentation algorithm. The performance of this algorithm was validated by comparing the automated choroidal thickness maps with manually segmented choroidal thickness maps. In order to determine whether a correlation existed between local choroidal thickness measurements and local choroidal vessel densities, we analyzed the relationship between the patterns of choroidal thickness measurements and the distributions of choroidal blood vessel densities in nonexudative AMD eyes with and without RPD.

## Methods

Between August 2013 and August 2014, patients with the diagnosis of nonexudative AMD were included in a prospective OCT study[30] at the Bascom Palmer Eye Institute. The study sought to analyze the performance of OCT as a tool to establish the presence of RPD. It was approved by the institutional review board (IRB) at the University of Miami Miller School of Medicine and was performed in accordance with Health Insurance Portability and Accountability Act of 1996 regulations. All patients signed an IRB-approved consent before OCT imaging was performed.

A prototype SS-OCT instrument (Carl Zeiss Meditec, Dublin, CA, USA), operating at 100-kHz and with a central wavelength of 1050 nm, was used in the study. Optical coherence tomography images were acquired covering a 12 × 12 mm retinal area (40° field of view) centered at the fovea using a raster scanning strategy composed of 512 B-scans with 512 A-scans per B-scan. Color fundus imaging was obtained using a fundus camera–based flash system (TRC-50DX; Topcon Medical Systems, Oakland, NJ, USA). Autofluorescence (AF) imaging and infrared (IR) reflectance imaging were acquired with a confocal scanning laser ophthalmoscopic system (Spectralis; Heidelberg Engineering, Heidelberg, Germany). We acquired AF images using an excitation wavelength of 488 nm and a detection wavelength of >500 nm. Infrared reflectance images were acquired using a wavelength of 820 nm.

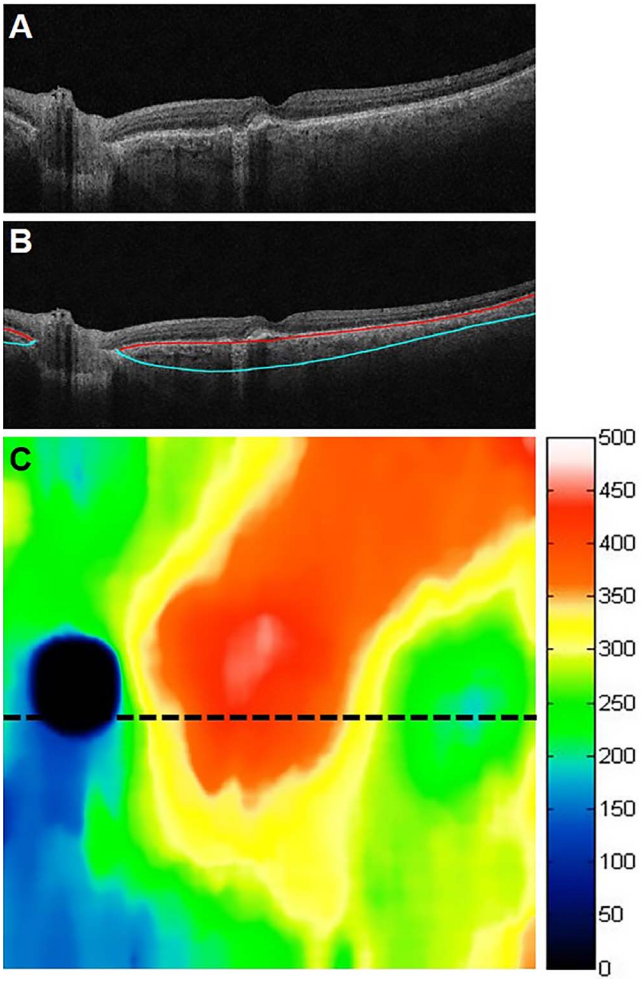


Figure 1. Automated choroidal segmentations and the corresponding choroidal thickness map. (**A**) B-scan through the fovea. (**B**) B-scan in **A** showing the automated segmentation lines: Bruch's membrane (*red line*) and the choroid/sclera interface (*blue line*). (**C**) Corresponding 12 × 12 mm choroidal thickness map with the associated color map in microns.

Eyes were partitioned into two groups based on a consensus assessment of whether RPD were present or absent based on standard multimodal fundus images, which included color, AF, and IR reflectance images, and en face OCT images generated using slabs with boundaries from 35 to 55 μm above the RPE as described previously by Schaal et al.[30] The original sample contained 88 nonexudative AMD eyes without RPD and 72 nonexudative AMD eyes with RPD. For the purposes of the current study, we reanalyzed a subset of the original dataset large enough to show a significant effect. We randomly selected 25 dry AMD eyes without RPD (group 1) and 25 dry AMD eyes with RPD (group 2) for this study.

A proprietary, fully automated custom segmentation algorithm was developed in a computing environment (MATLAB; MathWorks, Inc., Natick, MA, USA) to determine the anterior and posterior choroidal boundaries (i.e., Bruch's membrane and the choroidal/scleral interface). Choroidal thickness maps were generated from the OCT datasets of the eyes in the study (Fig. 1). In order to validate the performance of the choroidal segmentation algorithm, five eyes were randomly chosen from group 1, and five eyes were randomly chosen from group 2. Manual choroidal segmentation was performed by one of the authors [FZ] on all 512 B-scans from each of these 10 eyes by

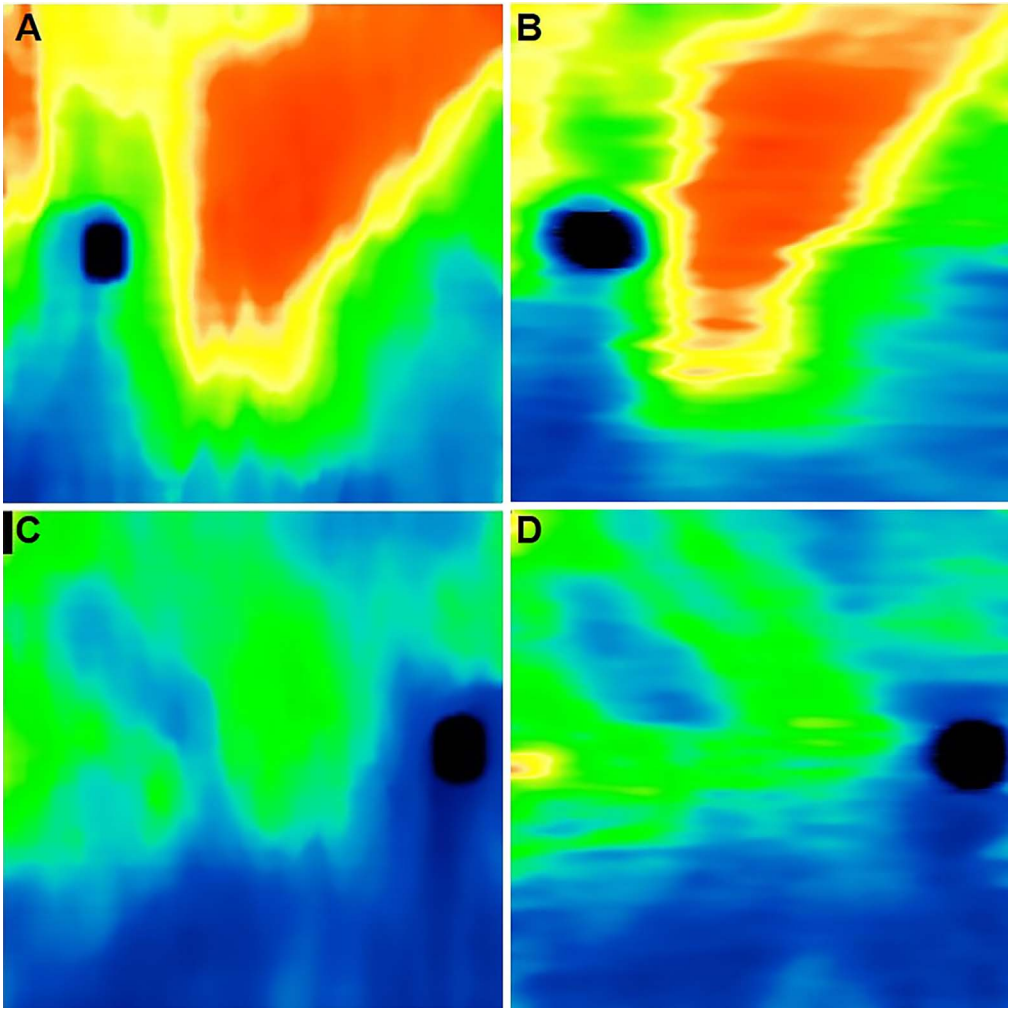


**Figure 2.** Comparison between (**A**, **C**) automated and corresponding (**B**, **D**) manual choroidal thickness maps. (**A**, **B**) *Top*: one eye without RPD. (**C**, **D**) *Bottom*: one eye with RPD.

using custom software. A comparison of the choroidal thickness maps obtained from the manual and automated segmentations in two of these eyes is shown in Figure 2.

In order to measure the choroidal vessel density, we used the automated algorithm to generate en face OCT choroidal slabs. The top boundary of the choroidal slab lay 40 μm below Bruch's membrane and the lower boundary was the choroidal/sclera interface. These choroidal slabs provide a good visualization of the large choroidal vessels (Fig. 3). Using intensity thresholding in a graphics editing software (Adobe Photoshop Elements 12; Adobe Systems, Inc., Mountain View, CA, USA), one of the authors (FZ) generated binary maps representing the distribution of the large choroidal vessels from the choroidal slabs (Fig. 3). Different local intensity thresholds were used to account for local variability in the relative intensities and contrast within the choroidal slabs. In addition, the optic disc region was removed from the resulting binary images. The choroidal vessel maps were generated without prior access to the corresponding choroidal thickness maps to avoid any possible influence on the results.

In order to quantify and compare choroidal thickness and choroidal vessel density, we defined a grid that resembled an Early Treatment Diabetic Retinopathy Study (ETDRS) target. The target was composed of an inner circle with a 1.5 mm radius and two concentric annular regions with radii of 3 and 6 mm, respectively. Each annular region was divided in four subfields: superonasal, superotemporal, inferonasal, and inferotemporal as shown in Figure 4. For each OCT image, the location of the fovea was determined manually as described previously[31] by examining the B-scans in both the horizontal and vertical directions. The ETDRS-like grid was then centered at the corresponding foveal location on both the choroidal thickness maps and the choroidal vessel maps. Vessel densities were computed from the binary vessel maps as the number of black pixel (vessels) in a given region divided the total number of pixels in that region.

## Results

The mean age of the nonexudative AMD eyes without RPD was 78.6 years (SD: 9.6), and the mean age of the nonexudative AMD eyes with RPD was 72.1 (SD: 8.3). Although choroidal thickness is typically thinner in nonexudative AMD eyes with RPD compared with nonexudative AMD eyes without RPD, we found that the specific thickness patterns varied significantly from eye to eye. Generally, the choroid was very thin in the inferonasal region as previously described[14] (Fig. 5). In the 10 eyes where manual segmentation was carried out, there was a good overall agreement between the manual and automated choroidal thickness maps (Fig. 2) with an average difference of 13.7 μm over the whole scan. A Bland-Altman plot of the

Investigative Ophthalmology & Visual Science

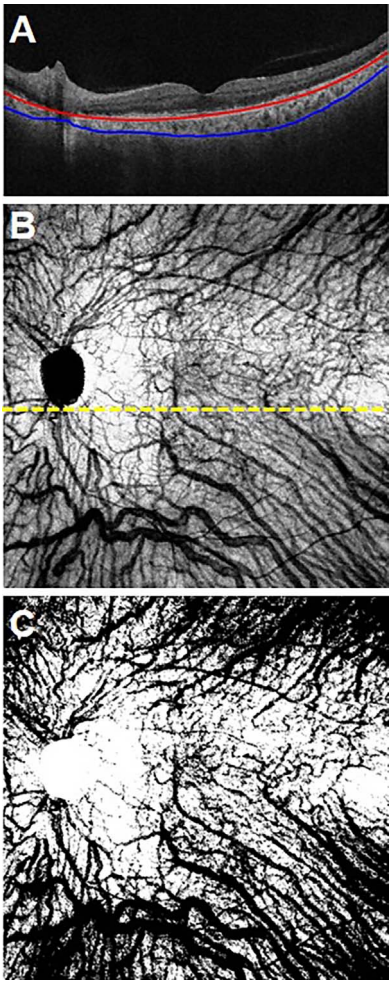


FIGURE 3. En face OCT choroidal slab and corresponding binary choroidal vessel density map. (**A**) A B-scan showing the automated choroidal segmentation lines. (**B**) The corresponding en face OCT choroidal slab. It spans from 40 μm below Bruch's membrane (*red line*) to the choroidal/scleral interface. (**C**) The binary choroidal maps generated from the slab in (**B**).

difference between the manual and automated choroidal thickness measurements for the 10 eyes over the 9 target subfields is shown in Figure 6. The automated choroidal thickness values are on average slightly larger than those obtained from the manual segmentations.

A qualitative overview of the choroidal thickness maps and the vessel density maps shown in Figure 7 suggested that, while there was a lot of variability in these maps—both within a given scan and across different eyes—there appeared to be a relationship between the patterns with a higher density of large choroidal vessels in areas with relatively larger choroidal thickness measurements. A quantitative representation of this relationship over the aggregate of the nine target subfields is shown in Figure 8. We found that larger choroidal thickness measurements did correlate with higher choroidal vessel densities, and this relationship was essentially the same for group 1 and group 2 study participants. However, group 2 did have thinner choroidal measurements and lower vessel densities overall. The correlation coefficient of choroidal thickness and choroidal vessel density was 0.77 for group 1 and 0.70 for group 2. There was no significant difference between the slope of the linear regressions in the two groups ($P = 0.66$). The overall relationship shown in Figure 8 is substantially stable over most of the single target subfield. Figure 9 shows the results for the central subfield comprised of a circle with a 3 mm diameter. The Table reports the average choroidal thickness measurements and vessel densities in the two groups for each subfield with choroidal thickness measurements significantly lower in group 2, except in the outer inferotemporal sector. Choroidal vessel densities were uniformly lower in group 2, although the difference did not always reach statistical significance, particularly in the outer inferonasal and inferotemporal sectors.

## Discussion

Understanding the choroidal geometry in both normal and diseased eyes could offer valuable information about the characteristics and progression of the underlying pathology. However, measurements of choroidal thickness limited to one or even several macular locations can only provide a very limited picture of the status of the choroid. In the last few years, several groups have generated choroidal thickness maps of various sizes either manually[6,29] or using automated algorithms.[23,32–37] Swept-source OCT imaging at longer wavelengths has several clear advantages over SD-OCT imaging, such as increased penetration through the RPE, decreased sensitivity roll-off, and higher scanning speeds, which enable larger areas to be scanned and/or higher A-scan density.[38] Therefore, SS-OCT provides the opportunity to generate wide-field choroidal thickness maps and enables the study of large-scale structures, such as the distribution of the large choroidal vessels and their association with the pattern of choroidal thickness measurements.

An overview of the choroidal thickness maps generated by automated choroidal segmentation algorithms in the literature shows that they tend to be affected by either artefactual discontinuities or by over-smoothing masking local variations, or both. The choroidal segmentation algorithm introduced in this report is an effort to overcome these problems and to generate a more realistic automated choroidal thickness map. The manual validation of the fully automated choroidal segmentation algorithm used a relatively small number of manually segmented eyes since manual segmentation of these OCT datasets is quite labor intensive, given the large number of B-scans. The automated results are shown to be close pointwise to the manually drawn boundaries and are able to capture the distribution patterns of local choroidal thickness measurements, at least in the eyes with dry AMD considered here (Fig. 2). Nevertheless, the possibility of artifacts is always a potential weakness in a study using automated segmentation.

Many factors can influence choroidal thickness, such as age, axial length, sex, blood pressure, eye pressure, and hypercholesterolemia.[3,39–42] Even some environmental factors such as drinking coffee or smoking can influence choroidal thickness.[43–45] It is not known how or whether these factors affect the local choroidal geometry, although it might be reasonable to assume that such systemic factors would have a global effect. However, it is likely that certain pathologies might cause localized changes in the distribution of choroidal thickness and choroidal vessels and these changes might be useful for monitoring different stages of disease progression.

Gerendas et al.[46] compared choroidal thickness measurements on a single central B-scan with the average choroidal thickness measurements over an ETDRS target. They found that the single B-scan measurements correlated well with the volumetric measurements in their sample of eyes. However, average choroidal thickness is a parameter that poorly describes the variability in the distribution of the choroidal thickness measurements we observed, particularly over larger

Investigative Ophthalmology & Visual Science

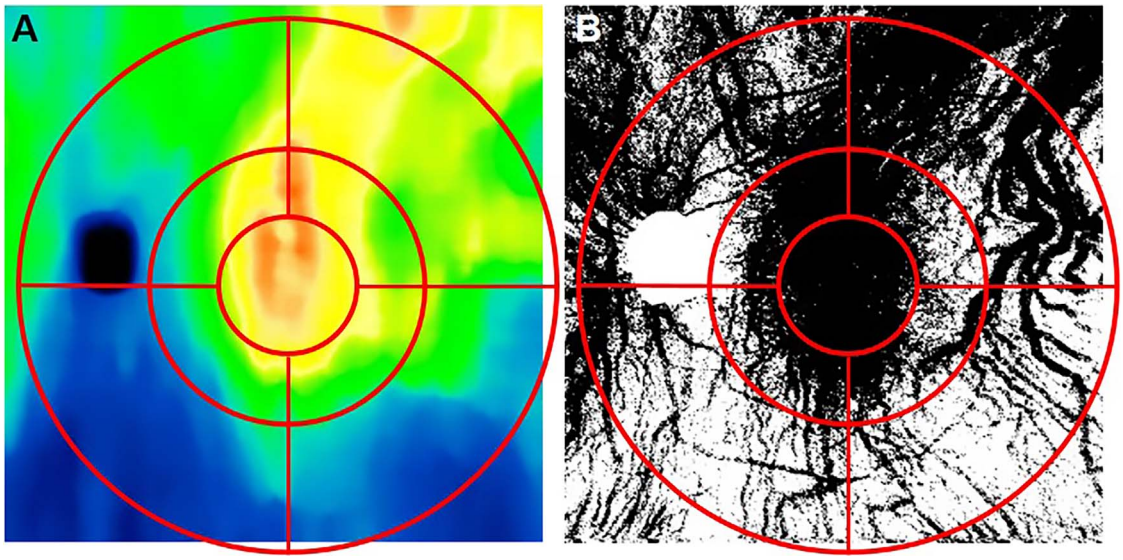


FIGURE 4. Early Treatment Diabetic Retinopathy Study–like grid used for subfield analyses of choroidal thickness measurements and choroidal vessel densities. (**A**) Overlay of grid on a choroidal thickness map. (**B**) Overlay of grid on a binary choroidal vessel density map. Grid consisted of 3-, 6-, and 12-mm diameter circles centered on the fovea.

retinal areas. For instance, it has been observed by several authors that the choroid is thinner in the region inferior and nasal to the optic disc,[4,21,34,47–49] which is probably the result of ocular development and closure of the optic cup. Clearly, central choroidal thickness could not be, in general, a good predictor of the wider distribution of choroidal thickness on this scale.

Haas et al.[19] analyzed wide-field SS-OCT choroidal maps of AMD patients and reported a correlation between local choroidal thickening and the geographic distribution of RPD within each eye and an overall thinning, which they attributed to AMD severity and the presence of RPD. This result is intriguing, but it is somewhat difficult to quantify such a correlation in a manner that takes into account other confounding factors. For instance, RPD are typically distributed preferentially at the superior and/or superior temporal arcades[26,50] and the distribution of choroidal thickness tends to be larger in these regions.[26,51] Our results give more information on the geographic distribution of choroidal thickness, confirming that average choroidal thickness is larger in superior sectors than in the corresponding inferior ones.

Using en face SS-OCT, Dansingani et al.[52] suggested that choroidal thickness maps correlated spatially with the distribution of dilated outer choroidal vessels in pachychoroid spectrum disorders. A recent work by Mohler et al.[29] analyzed SS-OCT choroidal thickness maps covering a 60° field of view.

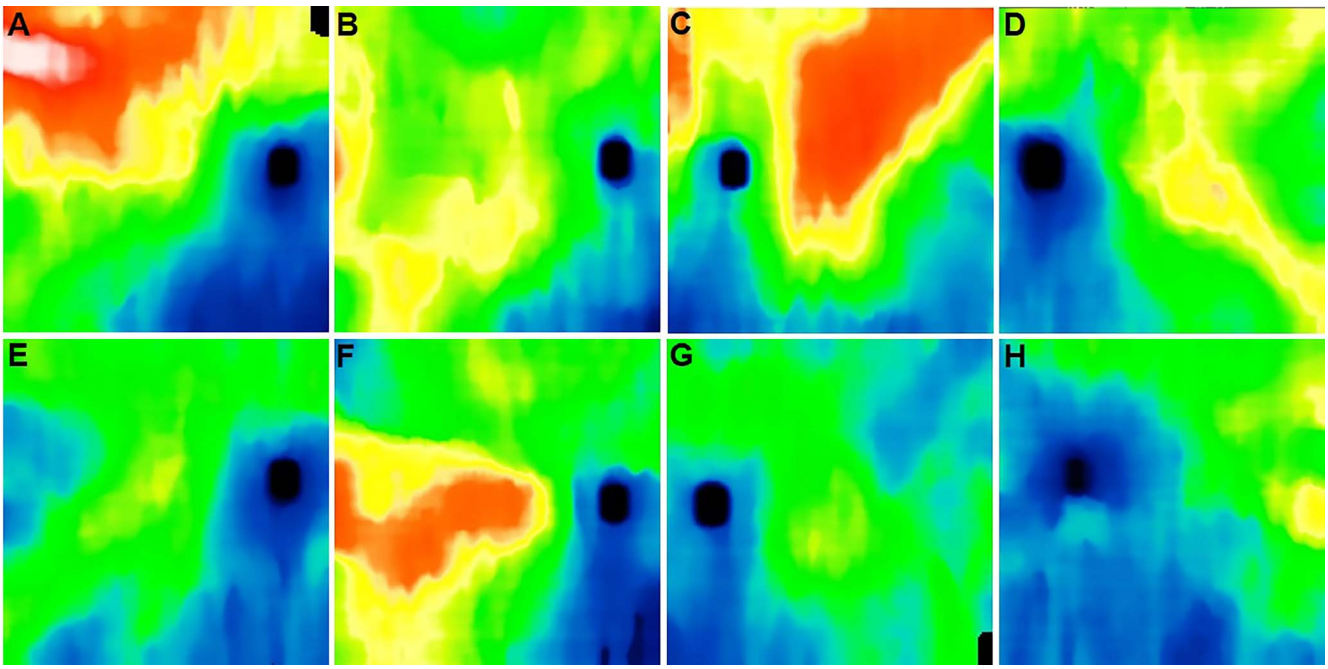


FIGURE 5. Examples of choroidal thickness maps of nonexudative AMD eyes with and without RPD. (**A–D**) Eyes with nonexudative AMD without RPD. (**E–H**) Eyes with nonexudative AMD with RPD.

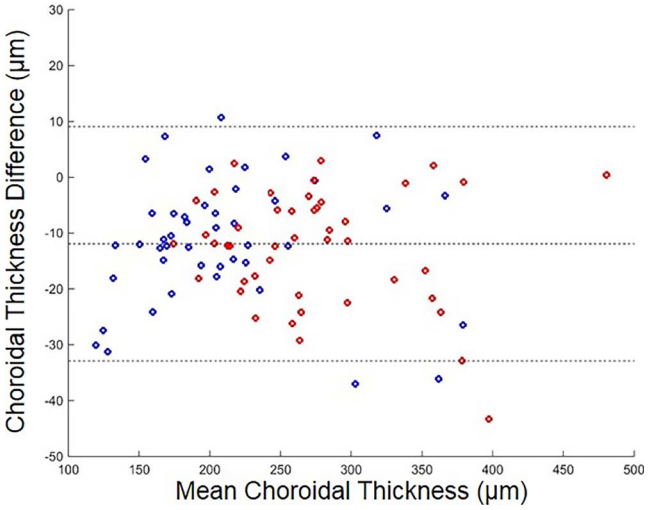


FIGURE 6. Bland-Altman plot of manual choroidal thickness measurements minus automated choroidal thickness measurements over all subfields. *Red*: group 1 without RPD. *Blue*: group 2 with RPD. The *dotted lines* show the mean difference and the 95% limits of agreement (mean difference ± 1.96 SD of the difference).

This was a purely descriptive study of a small number of eyes using manual segmentation. However, there was a suggestion that the choroidal vascular pattern might play a role in the distribution of choroidal thickness measurements. We similarly had noticed an apparent correspondence between choroidal thickness and choroidal vasculature patterns (Gregori G, et al. *IOVS* 2015;56:ARVO E-Abstract 5155), and we hypothesized that this correlation might be more apparent in eyes with AMD and RPD since the choroid is thinner in these eyes.

To the best of our knowledge, we report here the first quantitative analysis of the relationship between choroidal thickness and large choroidal vessels. Our results show that the choroid is thicker in regions with a higher density of large choroidal vessels in nonexudative AMD eyes, irrespective of whether RPDs are present. We found that the correlation between choroidal thickness and vessel density was essentially the same in the two samples in both the overall area and in targeted subfields, although the choroidal thickness was significantly lower in eyes with RPD. For instance, the Table shows that the average choroidal thickness is significantly lower in group 2 for all subfields except for the outer inferotemporal one. Moreover, the average and the distribution of choroidal thickness measurements in the central subfield in the two groups match those published by Thorell et al.[20] For both groups, average choroidal thickness in all superior sectors is larger than that in the corresponding inferior sectors (i.e., larger in the outer superotemporal sector than in outer inferotemporal sector, etc.). Correspondingly, in group 2, the choroidal vessel density is significantly lower in the aggregate, and uniformly lower in all subfields. This decrease in choroidal vessel density in eyes with nonexudative AMD and RPD is consistent with the hypothesis that RPD are a feature associated with an underlying vasculopathy. The relative small sample size is most likely responsible for the failure to achieve a significant difference in vessel density between the two groups over the interior inferotemporal and the outer superotemporal sectors. However, the reduction in average vessel density was small in the outer inferonasal and the outer inferotemporal sectors. This was not surprising for the outer inferonasal sector since this sector had the lowest average vessel density in all cases. It is not immediately obvious why the outer inferotemporal sector should behave differently from

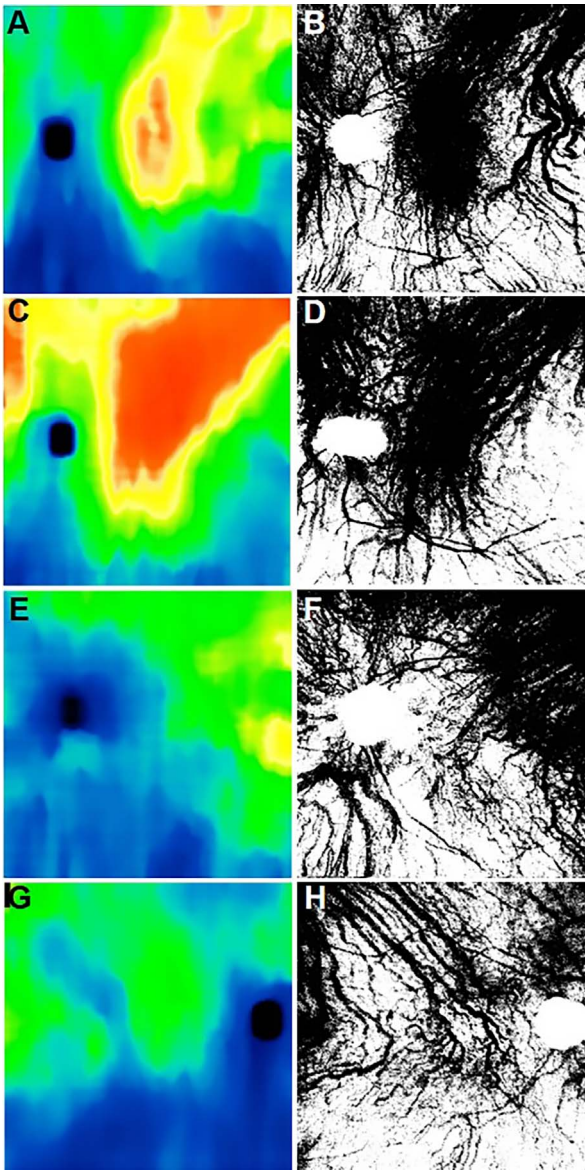


FIGURE 7. Examples of choroidal thickness maps with corresponding binary choroid vessel density maps with and without RPD. (**A**, **C**, **E**, **G**) Choroidal thickness maps. (**B**, **D**, **F**, **H**) Binary choroidal vessel density map. (**A**–**D**) Nonexudative AMD eye without RPD. (**E**–**H**) Dry AMD eyes with RPD.

all the others, and further investigation might be warranted. Nevertheless, for both groups, the relationship between thickness and vessel density in this sector remain essentially as illustrated in Figures 8 and 9. It is quite remarkable how stable the relationship between choroidal thickness and choroidal vessel density was across both groups and most locations (Figs. 8, 9). In our sample, the regression lines for both overall and single subfield data are almost identical to each other and across the two groups.

The approach we took to quantify the choroidal vasculature using a manual, local intensity thresholding of choroidal slabs has some weaknesses; however, there is no standard approach to quantify the choroidal vessel density. The major retinal vessels are included in the OCT choroidal slabs. Other OCT features, as well as differences in illumination, could also possibly affect local intensity and contrast in the choroidal slabs and therefore in the binary vessel map. However, the

Investigative Ophthalmology & Visual Science

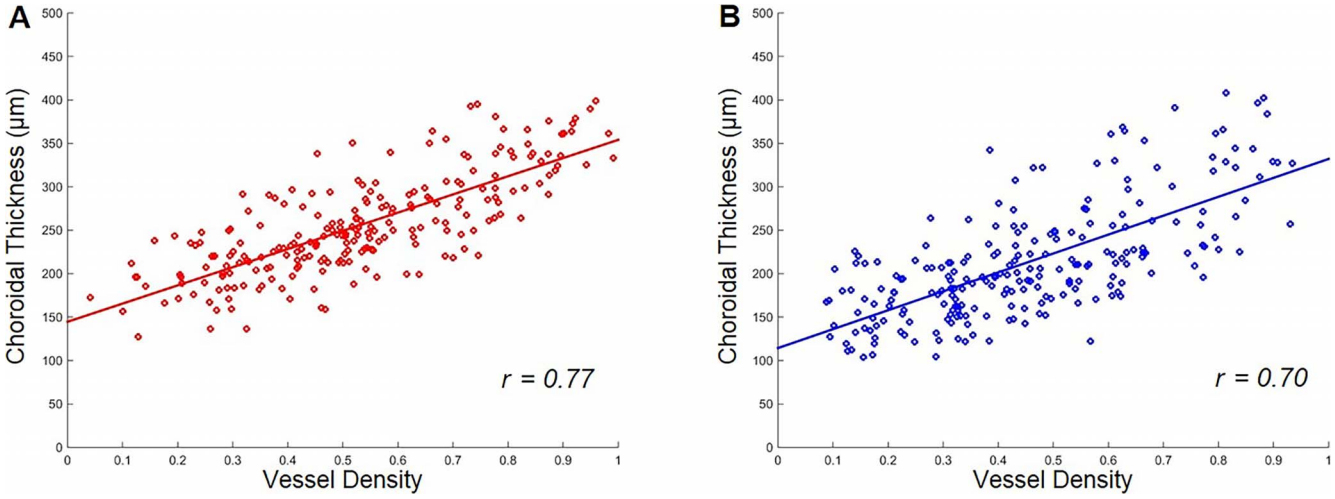


**Figure 8.** Plots of choroidal thickness measurements versus choroidal vessel density measurements over all subfields in eyes with and without RPD. (**A**) Group 1 without RPD ($r = 0.77$). (**B**) Group 2 with RPD ($r = 0.70$).

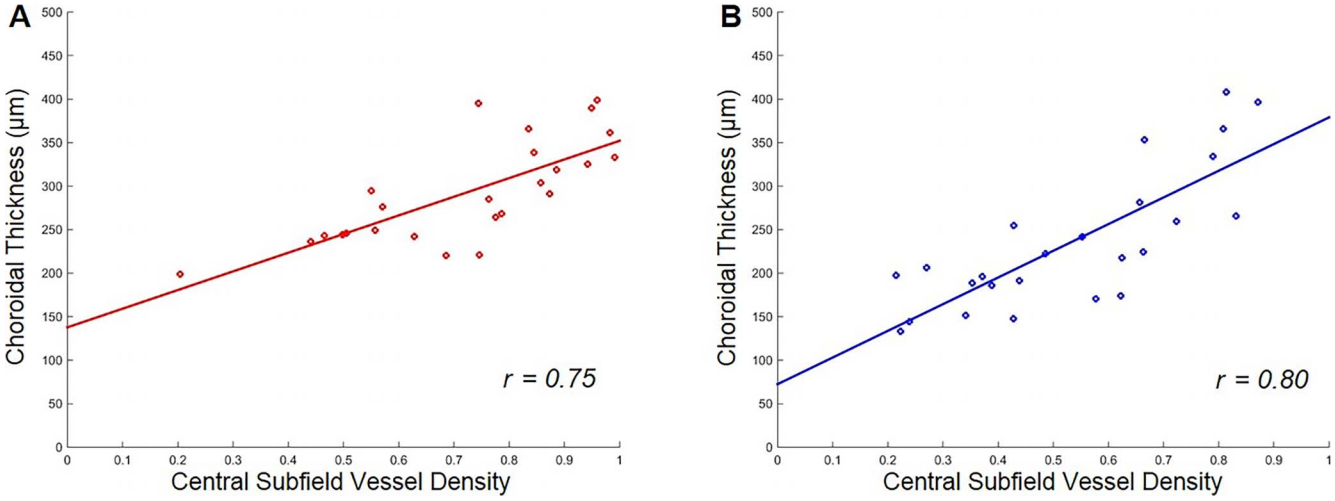


**Figure 9.** Plots of choroidal thickness measurements versus choroidal vessel density measurements over the central subfield in eyes with and without RPD. (**A**) Group 1 without RPD ($r = 0.75$). (**B**) Group 2 with RPD ($r = 0.80$).

relative contribution of the retinal vessels, the smaller choroidal vessels, and other factors to the vessel density is small compared with the contribution from the large choroidal vessels. We also introduced a new ETDRS-like target for the quantitation of choroidal vessels. An important note is that we divided the target into subfields using horizontal and vertical lines through the fovea (superotemporal, superonasal, inferotemporal, and inferonasal) rather than the more commonly seen superior, nasal, inferior, and temporal subfields. The reason for this choice was that the choroidal thickness patterns clearly followed a horizontal foveal divide, at least when it came to the inferonasal sector. Another issue is that the outer

**Table.** Average Choroidal Thickness (μm) and Vessel Density Across Subfields and Groups

| | Choroidal Thickness | | | Vessel Density | | |
|---|---|---|---|---|---|---|
| **Location** | **Group 1** | **Group 2** | ***P* Value** | **Group 1** | **Group 2** | ***P* Value** |
| Central subfield | 292.49 | 236.57 | 0.007 | 0.73 | 0.53 | <0.001 |
| Interior inferonasal | 242.29 | 195.96 | 0.008 | 0.48 | 0.36 | 0.05 |
| Interior superonasal | 264.75 | 207.91 | 0.003 | 0.58 | 0.40 | 0.002 |
| Interior superotemporal | 296.45 | 244.63 | 0.003 | 0.64 | 0.55 | 0.06 |
| Interior inferotemporal | 265.48 | 225.00 | 0.018 | 0.51 | 0.44 | 0.29 |
| Outer inferonasal | 185.54 | 160.59 | 0.023 | 0.32 | 0.31 | 0.75 |
| Outer superonasal | 225.58 | 182.91 | <0.001 | 0.52 | 0.44 | 0.01 |
| Outer superotemporal | 290.23 | 250.14 | 0.003 | 0.67 | 0.59 | 0.10 |
| Outer inferotemporal | 237.62 | 217.36 | 0.157 | 0.44 | 0.44 | 0.97 |
| All subfields | 255.60 | 213.45 | <0.001 | 0.55 | 0.45 | <0.001 |

circle in the target had a radius of 6 mm, and the target would not be entirely contained within the OCT scan if the scan was not perfectly centered at the fovea. In that case, some or all of the outer subfields may have been somewhat smaller than the corresponding sectors in the target. However, none of the eyes in our sample had any subfields missing more than 5% of the area from the corresponding sector. This should not have impacted our results since the averages were computed on the actual number of data points falling in the subfield.

Wide-field choroidal thickness maps may provide a better understanding of the choroidal thickness patterns and the physiologic factors that affect them. Given our results, as well as the examples shown by Mohler et al.,[29] it is likely that the patterns of choroidal vessels have an important effect on choroidal thickness, not only in normal eyes, but most notably in eyes with different ocular diseases. The profound association with RPD and the correlation between decreased vessel density and decreased choroidal thickness strongly suggest that the presence of RPD is a sign of an underlying choroidal vasculopathy. While it's possible that RPD could directly affect the choroidal vessel density, it seems more likely that they represent an underlying choroidal disease, especially since the location of RPDs do not correlate with the location of the thinnest choroid and the location with the lowest choroidal vessel density. More likely, RPDs represent a global ocular sign that there is an underlying vascular deficiency; however, much work remains to understand this relationship. In summary, wide-field SS-OCT imaging of the choroid is a useful strategy for identifying variations in choroidal thickness measurements, and these variations correlate with the density of the choroidal vessels.

## *Acknowledgments*

Supported by grants from Carl Zeiss Meditec, Inc.; the Macula Vision Research Foundation; the Emma Clyde Hodge Memorial Foundation; the Feig Family Foundation; an unrestricted grant from Research to Prevent Blindness, Inc.; a National Eye Institute Center Core grant (P30EY014801) to the Department of Ophthalmology, University of Miami Miller School of Medicine; the CAPES Foundation, Ministry of Education of Brazil, Brasília–Brazil (LR); and German Research Foundation Grant SCHA 1869/1-1 (KBS).

Disclosure: **F. Zheng**, None; **G. Gregori**, Carl Zeiss Meditec (F), P; **K.B. Schaal**, None; **A.D. Legarreta**, None; **A.R. Miller**, None; **L. Roisman**, None; **W.J. Feuer**, None; **P.J. Rosenfeld**, Achillion Pharmaceuticals (C), Acucela (C, F), Alcon (C), Apellis (F, I), Boehringer-Ingelheim (C), Carl Zeiss Meditec (C, F), Cell Cure Neurosciences (C), Chengdu Kanghong Biotech (C), CoDa Therapeutics (C), Digisight (I), Genentech (C, F), GlaxoSmithKline (F), Healios K.K (C), Hemera Biosciences (C), F. Hoffmann-La Roche Ltd. (C), MacRegen, Inc. (C), NGM Biopharmaceuticals (C), Neurotech (F), Ocata Therapeutics (C, F), Ocudyne (C), Regeneron (C), Stealth BioTherapeutics (C), Tyrogenex (C, F), Vision Medicines (C)

## *References*

1. Nickla DL, Wallman J. The multifunctional choroid. *Prog Retin Eye Res*. 2010;29:144–168.
2. Ferrara D, Waheed NK, Duker JS. Investigating the choriocapillaris and choroidal vasculature with new optical coherence tomography technologies. *Prog Retin Eye Res*. 2015;52:130–155.
3. Abbey AM, Kuriyan AE, Modi YS, et al. Optical coherence tomography measurements of choroidal thickness in healthy eyes: correlation with age and axial length. *Ophthalmic Surg Lasers Imaging Retina*. 2015;46:18–24.
4. Branchini LA, Adhi M, Regatieri CV, et al. Analysis of choroidal morphologic features and vasculature in healthy eyes using spectral-domain optical coherence tomography. *Ophthalmology*. 2013;120:1901–1908.
5. Yiu G, Pecen P, Sarin N, et al. Characterization of the choroid-scleral junction and suprachoroidal layer in healthy individuals on enhanced-depth imaging optical coherence tomography. *JAMA Ophthalmol*. 2014;132:174–181.
6. Barteselli G, Chhablani J, El-Emam S, et al. Choroidal volume variations with age, axial length, and sex in healthy subjects: a three-dimensional analysis. *Ophthalmology*. 2012;119:2572–2578.
7. Ozdogan Erkul S, Kapran Z, Uyar OM. Quantitative analysis of subfoveal choroidal thickness using enhanced depth imaging optical coherence tomography in normal eyes. *Int Ophthalmol*. 2014;34:35–40.
8. Goldenberg D, Moisseiev E, Goldstein M, Loewenstein A, Barak A. Enhanced depth imaging optical coherence tomography: choroidal thickness and correlations with age, refractive error, and axial length. *Ophthalmic Surg Lasers Imaging*. 2012;43:296–301.
9. Imamura Y, Fujiwara T, Margolis R, Spaide RF. Enhanced depth imaging optical coherence tomography of the choroid in central serous chorioretinopathy. *Retina*. 2009;29:1469–1473.
10. Maruko I, Iida T, Sugano Y, Go S, Sekiryu T. Subfoveal choroidal thickness in papillitis type of Vogt-Koyanagi-Harada disease and idiopathic optic neuritis. *Retina*. 2015;36:992–999.
11. Aoyagi R, Hayashi T, Masai A, et al. Subfoveal choroidal thickness in multiple evanescent white dot syndrome. *Clin Exp Optom*. 2012;95:212–217.
12. Coscas F, Puche N, Coscas G, et al. Comparison of macular choroidal thickness in adult onset foveomacular vitelliform dystrophy and age-related macular degeneration. *Invest Ophthalmol Vis Sci*. 2014;55:64–69.
13. Nunes RP, Goldhardt R, de Amorim Garcia Filho CA, et al. Spectral-domain optical coherence tomography measurements of choroidal thickness and outer retinal disruption in macular telangiectasia type 2. *Ophthalmic Surg Lasers Imaging Retina*. 2015;46:162–170.
14. Rhodes LA, Huisingh C, Johnstone J, et al. Peripapillary choroidal thickness variation with age and race in normal eyes. *Invest Ophthalmol Vis Sci*. 2015;56:1872–1879.
15. Ohsugi H, Ikuno Y, Oshima K, Tabuchi H. 3-D choroidal thickness maps from EDI-OCT in highly myopic eyes. *Optom Vis Sci*. 2013;90:599–606.
16. Kase S, Endo H, Yokoi M, et al. Choroidal thickness in diabetic retinopathy in relation to long-term systemic treatments for diabetes mellitus. *Eur J Ophthalmol*. 2015;26:158–162.
17. Galgauskas S, Laurinaviciute G, Norvydaite D, Stech S, Asoklis R. Changes in choroidal thickness and corneal parameters in diabetic eyes. *Eur J Ophthalmol*. 2015;26:163–716.
18. Mrejen S, Spaide RF. The relationship between pseudodrusen and choroidal thickness. *Retina*. 2014;34:1560–1566.
19. Haas P, Esmaeelpour M, Ansari-Shahrezaei S, Drexler W, Binder S. Choroidal thickness in patients with reticular pseudodrusen using 3D 1060-nm OCT maps. *Invest Ophthalmol Vis Sci*. 2014;55:2674–2681.
20. Thorell MR, Goldhardt R, Nunes RP, et al. Association between subfoveal choroidal thickness, reticular pseudodrusen and geographic atrophy in age-related macular degeneration. *Ophthalmic Surg Lasers Imaging Retina*. 2015;46:513–521.
21. Yun C, Oh J, Ahn SE, Hwang SY, Kim SW, Huh K. Peripapillary choroidal thickness in patients with early age-related macular degeneration and reticular pseudodrusen. *Graefes Arch Clin Exp Ophthalmol*. 2015;254:427–435.
22. Yiu G, Chiu SJ, Petrou PA, et al. Relationship of central choroidal thickness with age-related macular degeneration status. *Am J Ophthalmol*. 2015;159:617–626.

23. Esmaeelpour M, Kajic V, Zabihian B, et al. Choroidal Haller's and Sattler's layer thickness measurement using 3-dimensional 1060-nm optical coherence tomography. *PLoS One*. 2014;9: e99690.
24. Esmaeelpour M, Ansari-Shahrezaei S, Glittenberg C, et al. Choroid, Haller's and Sattler's layer thickness in intermediate age-related macular degeneration with and without fellow neovascular eyes. *Invest Ophthalmol Vis Sci*. 2014;55:5074–5080.
25. Esmaeelpour M, Brunner S, Ansari-Shahrezaei S, et al. Choroidal thinning in diabetes type 1 detected by 3-dimensional 1060 nm optical coherence tomography. *Invest Ophthalmol Vis Sci*. 2012;53:6803–6809.
26. Querques G, Querques L, Forte R, Massamba N, Coscas F, Souied EH. Choroidal changes associated with reticular pseudodrusen. *Invest Ophthalmol Vis Sci*. 2012;53:1258–1263.
27. Grewal DS, Chou J, Rollins SD, Fawzi AA. A pilot quantitative study of topographic correlation between reticular pseudodrusen and the choroidal vasculature using en face optical coherence tomography. *PLoS One*. 2014;9:e92841.
28. Vongkulsiri S, Ooto S, Mrejen S, Suzuki M, Spaide RF. The lack of concordance between subretinal drusenoid deposits and large choroidal blood vessels. *Am J Ophthalmol*. 2014;158: 710–715.
29. Mohler KJ, Draxinger W, Klein T, et al. Combined 60 degrees wide-field choroidal thickness maps and high-definition en face vasculature visualization using swept-source megahertz OCT at 1050 nm. *Invest Ophthalmol Vis Sci*. 2015;56:6284–6293.
30. Schaal KB, Legarreta AD, Gregori G, et al. Widefield en face optical coherence tomography imaging of subretinal drusenoid deposits. *Ophthalmic Surg Lasers Imaging Retina*. 2015;46:550–559.
31. Wang F, Gregori G, Rosenfeld PJ, Lujan BJ, Durbin MK, Bagherinia H. Automated detection of the foveal center improves SD-OCT measurements of central retinal thickness. *Ophthalmic Surg Lasers Imaging*. 2012;43:S32–S37.
32. Kajic V, Esmaeelpour M, Glittenberg C, et al. Automated three-dimensional choroidal vessel segmentation of 3D 1060 nm OCT retinal data. *Biomed Opt Express*. 2013;4:134–150.
33. Kajic V, Esmaeelpour M, Povazay B, Marshall D, Rosin PL, Drexler W. Automated choroidal segmentation of 1060 nm OCT in healthy and pathologic eyes using a statistical model. *Biomed Opt Express*. 2012;3:86–103.
34. Gerendas BS, Waldstein SM, Simader C, et al. Three-dimensional automated choroidal volume assessment on standard spectral-domain optical coherence tomography and correlation with the level of diabetic macular edema. *Am J Ophthalmol*. 2014;158:1039–1048.
35. Philip AM, Gerendas BS, Zhang L, et al. Choroidal thickness maps from spectral domain and swept source optical coherence tomography: algorithmic versus ground truth annotation. *Br J Ophthalmol*. 2016;100:1039–1048.
36. Zhang L, Buitendijk GH, Lee K, et al. Validity of automated choroidal segmentation in SS-OCT and SD-OCT. *Invest Ophthalmol Vis Sci*. 2015;56:3202–3211.
37. Zhang L, Lee K, Niemeijer M, Mullins RF, Sonka M, Abramoff MD. Automated segmentation of the choroid from clinical SD-OCT. *Invest Ophthalmol Vis Sci*. 2012;53:7510–7519.
38. Chinn SR, Swanson EA, Fujimoto JG. Optical coherence tomography using a frequency-tunable optical source. *Opt Lett*. 1997;22:340–342.
39. Li XQ, Larsen M, Munch IC. Subfoveal choroidal thickness in relation to sex and axial length in 93 Danish university students. *Invest Ophthalmol Vis Sci*. 2011;52:8438–8441.
40. Ahn SJ, Woo SJ, Park KH. Retinal and choroidal changes with severe hypertension and their association with visual outcome. *Invest Ophthalmol Vis Sci*. 2014;55:7775–7785.
41. Kubota T, Jonas JB, Naumann GO. Decreased choroidal thickness in eyes with secondary angle closure glaucoma. An aetiological factor for deep retinal changes in glaucoma? *Br J Ophthalmol*. 1993;77:430–432.
42. Wong IY, Wong RL, Zhao P, Lai WW. Choroidal thickness in relation to hypercholesterolemia on enhanced depth imaging optical coherence tomography. *Retina*. 2013;33:423–428.
43. Vural AD, Kara N, Sayin N, Pirhan D, Ersan HB. Choroidal thickness changes after a single administration of coffee in healthy subjects. *Retina*. 2014;34:1223–1228.
44. Zengin MO, Cinar E, Kucukerdonmez C. The effect of nicotine on choroidal thickness. *Br J Ophthalmol*. 2014;98:233–237.
45. Mansouri K, Medeiros FA, Marchase N, Tatham AJ, Auerbach D, Weinreb RN. Assessment of choroidal thickness and volume during the water drinking test by swept-source optical coherence tomography. *Ophthalmology*. 2013;120:2508–2516.
46. Gerendas BS, Hecht A, Kundi M, et al. Choroidal line scan measurements in swept-source optical coherence tomography as surrogates for volumetric thickness assessment. *Am J Ophthalmol*. 2016;162:150–158.e151.
47. Ho J, Branchini L, Regatieri C, Krishnan C, Fujimoto JG, Duker JS. Analysis of normal peripapillary choroidal thickness via spectral domain optical coherence tomography. *Ophthalmology*. 2011;118:2001–2007.
48. Huang W, Wang W, Zhou M, et al. Peripapillary choroidal thickness in healthy Chinese subjects. *BMC Ophthalmol*. 2013;13:23.
49. Tanabe H, Ito Y, Terasaki H. Choroid is thinner in inferior region of optic disks of normal eyes. *Retina*. 2012;32:134–139.
50. Alten F, Clemens CR, Heiduschka P, Eter N. Localized reticular pseudodrusen and their topographic relation to choroidal watershed zones and changes in choroidal volumes. *Invest Ophthalmol Vis Sci*. 2013;54:3250–3257.
51. Taban M, Sharma S, Williams DR, Waheed N, Kaiser PK. Comparing retinal thickness measurements using automated fast macular thickness map versus six-radial line scans with manual measurements. *Ophthalmology*. 2009;116:964–970.
52. Dansingani KK, Balaratnasingam C, Naysan J, Freund KB. En face imaging of pachychoroid spectrum disorders with swept-source optical coherence tomography. *Retina*. 2015;36:499–516.


Investigative Ophthalmology & Visual Science